KFUPM
Journal of Undergraduate Research International

Diamond Open Access 130

Article Mechanical Engineering

Thermally Driven Closed-air Open-water HDH System Integrated with Ejector Cooling System

Rand Almutairi and Obaidallah Munteshari*

Cite https://doi.org/10.64589/juri/231593

Submitted: April 19, 2026 **Revised:** May 03, 2026 **Accepted:** May 04, 2026

ABSTRACT

Conventional closed-air open-water (CAOW) humidification–dehumidification (HDH) desalination systems are attractive for small-scale freshwater production using low-grade thermal energy. However, their low thermal efficiency increases the required external heat input, limiting their application. This is mainly associated with insufficient internal heat recovery and weak thermal coupling between heating and condensation processes. A hybrid HDH configuration that integrates an air-heated CAOW HDH cycle with a thermally driven ejector cooling system (ECS) has been developed to improve the thermal performance of the cycle. The novelty of this study is the dual thermal coupling strategy, which combines direct air-loop heating with feedwater precooling within a single integrated HDH–ECS configuration. Mass and energy balance equations were formulated for every system component and assembled into a steady-state thermodynamic model, which was implemented and solved in Engineering Equation Solver (EES). The model was validated against published HDH data, with the predicted gained output ratio deviating by less than 1% under the same operating conditions. The effects of mass ratio, top air temperature, and ejector operating temperatures on system performance were investigated using parametric analyses. The integrated system enhanced the peak gained output ratio of the standalone HDH cycle by approximately 41.8%. The maximum recovery ratio of the hybrid system reached 3.3%. Results showed that entrainment ratio is a key thermal-improvement parameter, with evaporator and condenser temperatures exerting the strongest influence on performance. The proposed HDH–ECS configuration can improve CAOW desalination efficiency using low-grade thermal energy.

Keywords: desalination, humidification–dehumidification, closed-air open-water system, ejector cooling system, thermal efficiency

1. INTRODUCTION

The growing global demand for freshwater and energy presents one of the most critical sustainability challenges of the modern era. Global water demand and energy consumption are both projected to rise substantially in the coming years[1,2]. These trends highlight the need for sustainable technologies that address both water scarcity and rising energy consumption.

Among the available technologies for addressing freshwater scarcity, humidification–dehumidification (HDH) desalination has emerged as a promising option due to its simple design, operational flexibility, and suitability for decentralized small-scale applications. One of the key advantages of HDH systems is their ability to utilize renewable thermal energy and other low-grade heat sources, making them attractive for off-grid and remote locations[3]. Several HDH configurations have been investigated in the literature, including open-air open-water (OAOW), closed-air open-water (CAOW), closed-water open-air (CWOA), and closed-air closed-water systems, each characterized by different balances between productivity, thermal performance, and system complexity[4]. In addition to producing potable water from saline resources, HDH systems offer practical benefits such as simplified brine handling, reduced pretreatment requirements, and relatively straightforward operation and maintenance[4]. Despite these advantages, conventional HDH systems are generally characterized by modest thermal efficiency, with reported gained output ratio (GOR) values typically ranging from 2 to 6 depending on the configuration and operating conditions[4,5]. Consequently, considerable effort has been devoted to developing hybrid HDH configurations that improve internal heat recovery and reduce the need for external thermal energy input.

Numerous studies have focused on improving both the performance and predictive accuracy of HDH desalination systems. For example, a steady-state mathematical model was developed to investigate heat and mass transfer mechanisms within HDH system components[5]. Narayan et al. conducted a thermodynamic assessment of different HDH cycle configurations and proposed alternative arrangements aimed at improving thermal efficiency, with emphasis on conventional HDH systems rather than hybrid configurations[4]. Farsad and Behzadmehr[6] analyzed a solar-driven HDH desalination unit using numerical

Published under an exclusive license by KFUPM

mass and energy balance calculations together with design-of-experiments-based sensitivity analyses to identify favorable operating conditions. More recently, Mahmoudi et al.[7] reviewed a wide range of performance enhancement approaches for HDH systems, including multistage designs, bubble-column humidifiers, phase-change materials, nanofluids, ultrasonic humidification, thermoelectric integration, air saturators, fogging techniques, and desiccant-assisted processes. Similarly, Ziauddin et al.[8] introduced a solar-powered HDH system incorporating a low-energy ultrasonic atomizer to improve evaporation within the humidifier, highlighting the potential of atomization-assisted humidification for enhancing solar-driven HDH desalination performance.

The ejector cooling system (ECS) has attracted considerable attention as an energy-efficient cooling technology capable of utilizing low-grade and waste-heat sources without the need for mechanical compression. Previous studies have investigated different aspects of ECS performance, including mathematical modeling, thermodynamic analysis, and system optimization. He et al.[9] presented a comprehensive review of ejector modeling approaches, describing the underlying flow mechanisms and summarizing various formulations developed for ejector systems. Khaldi et al.[10] examined the thermodynamic performance of ejector refrigeration systems and evaluated the influence of operating conditions and refrigerant selection, including a comparison between R134a and the environmentally friendly refrigerant R1234yf. In addition, Khennich et al.[11] developed a steady-state model of a solar-powered ECS and assessed its performance under realistic operating conditions using solar thermal energy as the driving source. More recently, Yadav et al.[12] reviewed recent developments in solar-driven ejector refrigeration and multigeneration systems, emphasizing the roles of cycle modification, hybrid system integration, working-fluid selection, solar collector coupling, thermal-energy storage, and data-driven modeling in advancing future ECS technologies.

The integration of HDH desalination with ejector cooling technology has recently received increasing attention as a means of simultaneously improving freshwater production and thermal-energy utilization. Al-Mahmoud et al[13] investigated the thermodynamic performance of a hybrid HDH–ejector desalination system and demonstrated the feasibility of combining the two technologies for concurrent water and cooling production. Building on this concept, Ali et al.[14] proposed a solar-driven adsorption desalination–HDH configuration and reported improvements in freshwater productivity, thermal utilization, and environmental performance. In addition, recent review studies have identified hybrid HDH systems as a promising approach for improving desalination efficiency through the integration of multiple thermally coupled processes[15]. A related study employed a thermally driven ejector cooling system using R141b in conjunction with a water-heated HDH cycle and reported a GOR improvement of approximately 42%[16]. Nevertheless, the available hybrid HDH–ejector studies have primarily focused on water-heated configurations. In contrast, the present work investigates an air-heated CAOW HDH system using R134a, where the ejector condenser replaces the conventional air heater and the ejector evaporator simultaneously precools the feedwater supplied to the dehumidifier. Therefore, the novelty of this study lies in proposing a dual thermal coupling strategy that combines direct air-loop heating and feedwater precooling within a single CAOW HDH–ECS configuration. To the best of our knowledge, this configuration has not been comprehensively investigated in previous studies. Consequently, the combined effects of mass ratio, top air temperature, generator temperature, condenser temperature, and evaporator temperature on GOR, recovery ratio, freshwater production, and ejector entrainment ratio remain unclear. We address this gap by developing and validating a thermodynamic model of the proposed system and evaluating its performance under different operating conditions.

The primary objective of this study is to develop a steady-state thermodynamic model of the proposed hybrid HDH–ECS and to perform a parametric analysis of the effects of key operating parameters on system performance. Therefore, this study evaluates the influence of mass ratio and top air, generator, condenser, and evaporator temperatures on the gained output ratio, recovery ratio, freshwater production, and ejector entrainment ratio. The results are intended to clarify the thermodynamic behavior of the proposed configuration and highlight its potential for sustainable desalination using low-grade thermal energy. The scope of this study is limited to a steady-state thermodynamic-performance assessment; detailed exergy, environmental, and techno-economic analyses are beyond the scope of this study and are recommended for future work.

2. SYSTEM DESCRIPTION

Figure 1 presents the configuration of the CAOW HDH desalination cycle. The system operates with a closed air loop and an open water loop. Air entering the humidifier at state a_1 comes into contact with saline water, resulting in simultaneous heat and mass transfer. As moisture evaporates into the air stream, both its humidity ratio and enthalpy increase, and the air exits the humidifier at state a_2. The air is subsequently heated to state a_3 before entering the dehumidifier. Within the dehumidifier, cooling of the moist air causes part of the water vapor to condense and be collected as freshwater (pw), while the air leaves at state a_1 and recirculates through the system. On the water side, feedwater enters the dehumidifier at state w_0, gains heat from the moist air and leaves at state w_1 before flowing to the humidifier. Following partial evaporation in the humidifier, the remaining concentrated stream exits the system as brine at state w_2.

Figure 2 shows the thermally driven ejector cooling cycle using R134a as the refrigerant. Unlike conventional vapor-compression systems, the ejector replaces the mechanical compressor and enables the cycle to be driven by thermal energy. Heat supplied to the generator produces a high-pressure refrigerant vapor that enters the ejector as the primary stream at state r_1. As this stream expands through the nozzle, a low-pressure region is created, drawing in the secondary vapor stream from the evaporator at state r_5. The two streams mix within the ejector and are discharged at the condenser pressure. In the condenser, heat is rejected to the surroundings, and the refrigerant condenses into a liquid at state r_3. Part of the liquid is pumped to the generator, whereas the remaining portion is expanded through the throttling valve before entering the evaporator. The refrigerant then

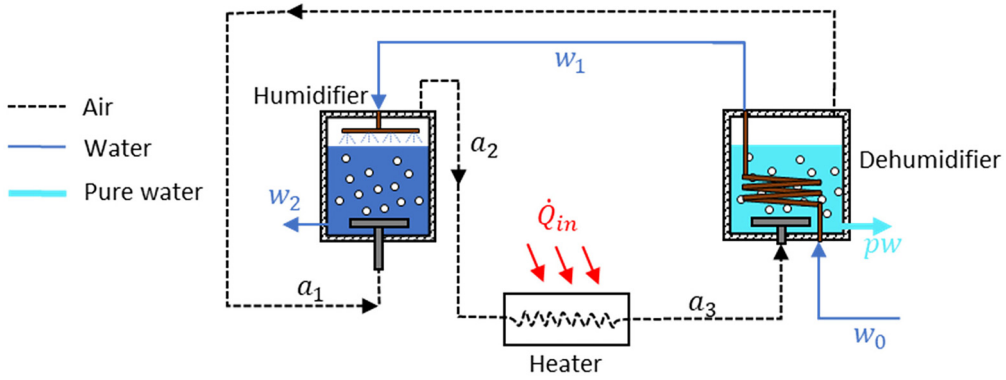

Figure 1. Schematic of CAOW air-heating HDH cycle

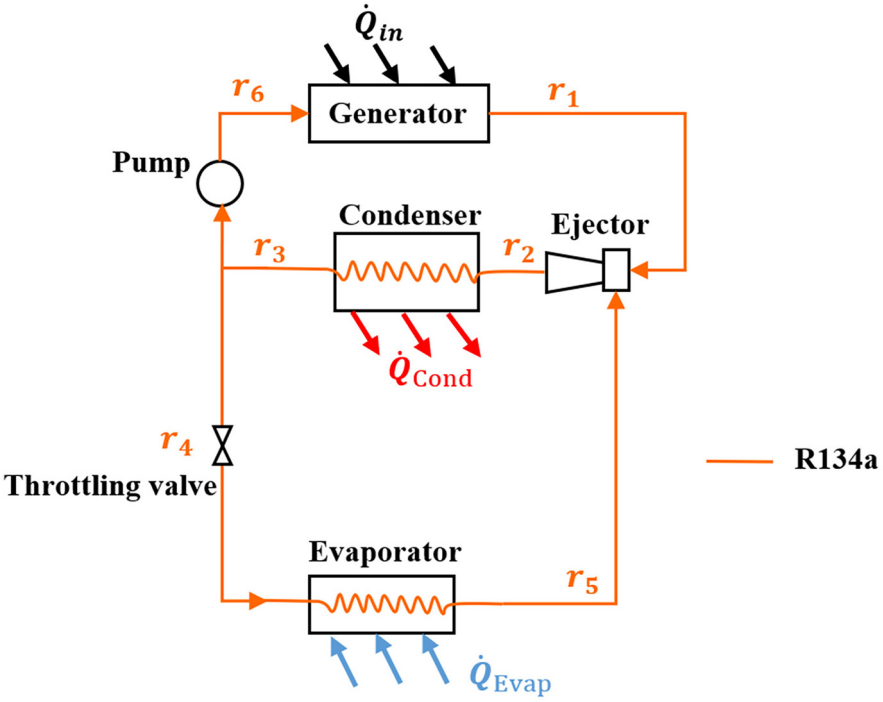

Figure 2. Schematic of ejector cooling cycle

absorbs heat in the evaporator, generating the cooling effect, and returns to the ejector to complete the cycle. Consequently, the heat released in the condenser is equal to the combined heat input to the generator and the heat absorbed in the evaporator, as represented by Eq. (1):

$$\dot{Q}_{cond} = \dot{Q}_{gen} + \dot{Q}_{evap} + \dot{W}_{pump} \quad (1)$$

Figure 3 presents the proposed hybrid HDH–ECS configuration. In this system, the condenser of the ejector cooling cycle replaces the conventional external air heater used in the standalone CAOW HDH system. Heat released during refrigerant condensation is transferred directly to the circulating air stream between the humidifier and dehumidifier, increasing the air temperature from state a_2 to state a_3 while maintaining a constant humidity ratio. At the same time, the evaporator extracts heat from the feedwater before it enters the dehumidifier. This arrangement strengthens the temperature difference driving condensation and consequently increases freshwater production. Similar approaches have been highlighted in previous HDH enhancement studies, which emphasize the role of improved internal heat recovery and favorable thermal integration in increasing desalination efficiency [13].

Unlike the conventional HDH cycle, where thermal energy is supplied directly to the air or water stream, the proposed configuration incorporates an additional internal heat-recovery pathway. The heat delivered to the air stream in the condenser originates from both the external energy supplied to the generator and the energy absorbed by the refrigerant in the evaporator, as indicated by Eq. (1). Although the feedwater is cooled before entering the dehumidifier, this cooling effect is offset because the absorbed energy is subsequently recovered at a higher temperature level in the condenser and transferred back to the HDH cycle. As a result, the integrated configuration utilizes thermal energy more effectively and achieves superior performance compared with the conventional CAOW HDH system.

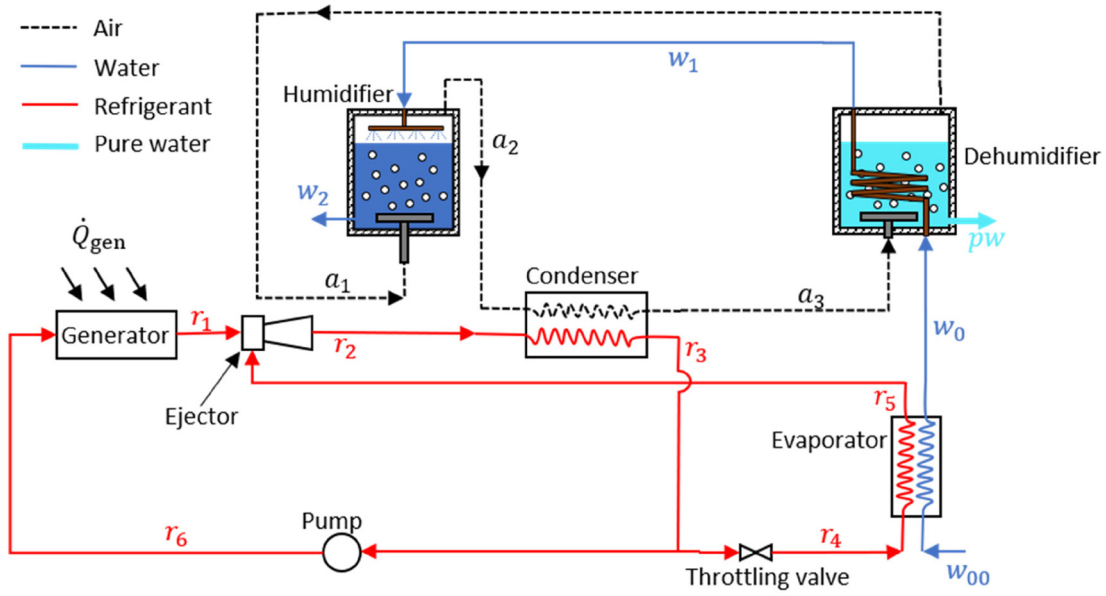

Figure 3. Schematic of the proposed HDH-ECS system

3. THERMODYNAMIC MODEL

The thermodynamic model of the proposed hybrid HDH–ECS is developed and solved using the EES. The model is formulated based on steady-state mass and energy balance equations applied to each component of the HDH desalination cycle and the ejector cooling cycle, as well as their thermal coupling in the integrated configuration.

The working fluids considered in the analysis include moist air, saline water, pure (fresh) water, and R134a as the refrigerant in the ejector cooling cycle. Thermophysical properties of R134a are obtained from the built-in EES refrigerant property database, while the properties of water and moist air are evaluated using standard correlations available within the solver. The coupled nonlinear equations governing the system behavior are solved iteratively until convergence is achieved for all thermodynamic state variables.

To evaluate the theoretical performance of the proposed hybrid HDH–ECS, the thermodynamic model is developed based on the following assumptions:

- The system operates under steady-state conditions.
- The system is perfectly insulated, and heat losses to the surroundings are negligible.
- Pressure drops in pipes and system components are negligible.
- Changes in kinetic and potential energy are negligible.
- The ambient air–water vapor mixture is treated as an ideal gas, and Dalton's law applies.
- The ambient air entering the system and the saline feedwater are assumed to enter at the same ambient temperature.
- Heating the air stream in the condenser is assumed to occur without any change in humidity ratio; therefore, the air humidity ratio remains constant during this process.
- In the dehumidifier, condensation occurs progressively as the humid air is cooled, and the condensate temperature is expected to lie between the inlet and outlet humid-air temperatures. Since the study adopts a lumped steady-state thermodynamic model rather than a spatially resolved heat-and-mass-transfer model, the freshwater outlet temperature is approximated as the arithmetic mean of the inlet and outlet humid-air temperatures. This simplified assumption was adopted in previous HDH–ejector thermodynamic modeling[16] and is used in this study to close the dehumidifier energy balance[4]:

$$T_{pw} = \frac{T_{a1} + T_{a3}}{2} \tag{2}$$

- Mixing of the primary and secondary refrigerant streams inside the ejector occurs at constant pressure.
- The refrigerant leaving the generator and the evaporator is treated as saturated vapor.
- At the condenser outlet, the refrigerant is taken to be saturated liquid.
- The compressed mixture is assumed to leave the ejector with negligible velocity.
- Within the ejector, the working fluid is modeled as an ideal gas.
- The effectiveness of the humidifier and that of the dehumidifier are selected as design parameters. The ejector entrainment ratio is determined from the ejector thermodynamic model.

3.1. Humidifier. In the humidifier, the circulating air stream comes into direct contact with the saline water stream, resulting in simultaneous heat and mass transfer between the two phases. During this process, part of the saline water evaporates into the air stream, increasing both the humidity ratio and specific enthalpy of the air. The remaining water leaves the humidifier as a concentrated brine stream. The mass and energy balance equations governing the humidifier are given by[4]

$$\dot{m}_b = \dot{m}_w - \dot{m}_{da}\,(\omega_{a2} - \omega_{a1}) \tag{3}$$

$$\dot{m}_w h_{w1} - \dot{m}_b h_{w2} = \dot{m}_{da}\,(h_{a2} - h_{a1}) \tag{4}$$

where h denotes the specific enthalpy and ω represents the humidity ratio, defined as the mass of water vapor per unit mass of dry air. The flow rates $\dot{m}_w$, $\dot{m}_b$, and $\dot{m}_{da}$ correspond to the

saline water, brine, and dry-air streams, respectively. The subscripts w, a, and r refer to the thermodynamic states of water, air, and refrigerant streams shown in Figure 3. In both systems, the saline feedwater is supplied at ambient temperature; this inlet temperature is denoted T_{w0} for the standalone system (Figure 1) and T_{w00} for the hybrid system (Figure 3).

The humidifier effectiveness is defined as the ratio between the actual enthalpy change and the maximum attainable enthalpy change within the humidifier. Following Narayan et al.[4], the humidifier effectiveness ε_H is expressed as

$$\varepsilon_H = \max\left[\frac{h_{a2}-h_{a1}}{h_{a2}^{ideal}-h_{a1}},\ \frac{h_{w1}-h_{w2}}{h_{w1}-h_{w2}^{ideal}}\right] \tag{5}$$

where h_{a2}^{ideal} represents the maximum attainable humid-air enthalpy obtained when the outlet-air temperature approaches the inlet-water temperature $\left(T_{a2}^{ideal}=T_{w1}\right)$. Similarly, h_{w2}^{ideal} represents the minimum attainable brine enthalpy, obtained when the outlet-brine temperature approaches the wet-bulb temperature of the inlet air $\left(T_{w2}^{ideal}=T_{a1,wb}\right)$ [4]. A humidifier effectiveness of 0.90 was adopted in the present study, consistent with values commonly reported in the HDH literature. Higher humidifier effectiveness enhances heat and mass transfer between the two streams and therefore improves the overall performance of the system.

3.2. Dehumidifier. In the dehumidifier, the humid air stream is cooled indirectly by the incoming saline feedwater without any direct contact between the two streams. As the air temperature decreases, part of the water vapor condenses and is collected as distilled water at a rate of $\dot{m}_{pw}$. The mass and energy balance equations describing the dehumidifier are given by[4]

$$\dot{m}_{pw} = \dot{m}_{da}\left(\omega_{a3}-\omega_{a1}\right) \tag{6}$$

$$\dot{m}_w\left(h_{w1}-h_{w0}\right)+\dot{m}_{pw}h_{pw} = \dot{m}_{da}\left(h_{a3}-h_{a1}\right) \tag{7}$$

The dehumidifier effectiveness ε_D is defined as the ratio of the actual enthalpy change to the maximum possible enthalpy change, and it can be expressed as[4]

$$\varepsilon_D = \max\left[\frac{h_{a3}-h_{a1}}{h_{a3}-h_{a1}^{ideal}},\ \frac{h_{w1}-h_{w0}}{h_{w1}^{ideal}-h_{w0}}\right] \tag{8}$$

where h_{a1}^{ideal} denotes the minimum attainable enthalpy of the outlet air when its temperature approaches the inlet-water temperature $T_{a1}^{ideal}=T_{w0}$. Likewise, h_{w1}^{ideal} represents the maximum attainable enthalpy of the outlet water when its temperature approaches the inlet-air temperature $T_{w1}^{ideal}=T_{a3}$ [4]. A dehumidifier effectiveness of 0.90 was assumed in the present study, consistent with values commonly adopted in HDH desalination analyses. Increasing dehumidifier effectiveness enhances heat recovery and promotes water vapor condensation, resulting in higher freshwater production and improved overall system performance.

3.3. Condenser. Within the proposed CAOW HDH–ECS configuration, the condenser serves as the thermal link between the ejector cooling cycle and the HDH cycle. Heat released by the condensing refrigerant is transferred directly to the circulating air stream, increasing its temperature from state a_2 (humidifier outlet) to state a_3 (dehumidifier inlet) while maintaining a constant humidity ratio. At the same time, the evaporator cools the feedwater before it enters the dehumidifier, which enhances the condensation potential and contributes to higher freshwater production. Based on these interactions, the condenser energy balance can be expressed as

$$\dot{Q}_{cond} = \left(\dot{m}_{gen}+\dot{m}_{evap}\right)\left(h_{r2}-h_{r3}\right) = \dot{m}_{da}\left(h_{a3}-h_{a2}\right) \tag{9}$$

where $\dot{m}_{gen}$ and $\dot{m}_{evap}$ denote the refrigerant mass flow rates leaving the generator and evaporator, respectively, while the corresponding air states at the condenser inlet and outlet are represented by a_2 and a_3.

3.4. Evaporator. The evaporator extracts heat from the incoming feedwater before it enters the dehumidifier. This cooling process increases the temperature difference between the humid air and feedwater within the dehumidifier, thereby promoting condensation and improving freshwater production. The energy balance for the evaporator can be written as

$$\dot{Q}_{evap} = \dot{m}_{evap}\left(h_{r5}-h_{r4}\right) = \dot{m}_w\left(h_{w00}-h_{w0}\right) \tag{10}$$

3.5. Generator. The generator is the only component that receives external thermal energy in the proposed system. Heat supplied to the generator vaporizes the refrigerant and produces the high-pressure motive vapor required for ejector operation. The generator energy balance is given by

$$\dot{Q}_{gen} = \dot{m}_{gen}\left(h_{r1}-h_{r6}\right) \tag{11}$$

3.6. Pump and Throttling Valve. After condensation, the refrigerant leaves the condenser as a saturated liquid at state r_3. A portion of this liquid is pressurized by the pump to the generator pressure (state r_6), while the remaining portion is expanded through the throttling valve to the evaporator pressure (state r_4). The pump work and throttling process are described by

$$\dot{W}_{pump} = \dot{m}_{gen}\left(h_{r6}-h_{r3}\right) \tag{12}$$

$$h_{r4} = h_{r3} \tag{13}$$

3.7. Ejector. The ejector is the key component of the ejector cooling cycle, where the primary refrigerant stream from the generator interacts with the secondary stream from the evaporator. Expansion of the high-pressure primary vapor through the nozzle creates a low-pressure region that entrains the secondary vapor. The two streams mix within the ejector and are discharged at an intermediate pressure suitable for condensation. The ejector mass balance is expressed as[18]

$$\dot{m}_{gen}+\dot{m}_{evap} = \dot{m}_{cond} \tag{14}$$

The ejector performance is characterized by the entrainment ratio μ, defined as the ratio of the secondary to primary mass flow rates[18]

$$\mu = \frac{\dot{m}_{evap}}{\dot{m}_{gen}} \tag{15}$$

The ejector is modeled using a one-dimensional constant-pressure mixing formulation with nozzle and diffuser isentropic efficiency corrections, consistent with approaches commonly adopted in ejector refrigeration studies[18,19]. The formulation is based on the Munday–Bagster model, which has been widely

applied and validated for the analysis of ejector refrigeration systems [18].

In the ejector, saturated refrigerant vapor from the generator enters at high pressure and temperature (r_1) and expands through the convergent–divergent nozzle to the evaporator pressure, P_{evap}, reaching state (a). The nozzle performance is represented by the isentropic efficiency η_{nozz}. The secondary saturated vapor stream enters the ejector from the evaporator at state (r_5) and at the same pressure level, P_{evap}. The two streams mix within the ejector under the assumption of constant-pressure mixing, an approach that has been shown to provide reliable predictions for ejector performance [19]. Following the mixing process, the combined flow is compressed in the diffuser and exits the ejector at state r_2. The diffuser performance is characterized by the isentropic efficiency η_{diff}. The entrainment ratio and the refrigerant enthalpy at the ejector outlet are the primary variables used to evaluate ejector performance and are determined through the iterative solution procedure described below.

Following the one-dimensional ejector model formulation [18,19]. The solution procedure is initiated by assuming an initial value for the entrainment ratio, μ. An initial estimate of the ejector outlet enthalpy, h_{r2}, is then obtained from the ejector energy balance

$$h_{r1} + \mu h_{r5} = (1 + \mu)\, h_{r2} \tag{16}$$

Because the velocity of the primary stream at the nozzle inlet, v_{r1}, is negligible compared with the nozzle exit velocity, v_a, the latter can be evaluated from the energy conservation equation. Likewise, the velocity at state (b) after the mixing process can be determined using stagnation enthalpy. Under the assumption of constant-pressure mixing, application of the momentum conservation equation in the mixing chamber gives the static enthalpy at state (b) as [19]

$$h_b = h_{r2} - \frac{(h_{r1} - h_a)}{(1 + \mu)^2} \tag{17}$$

The nozzle exit condition is evaluated using the isentropic expansion relationships together with the nozzle efficiency correction typically employed in ejector refrigeration analyses [18,20]. The actual enthalpy at the nozzle exit state (a), h_a, is obtained by applying the isentropic expansion process from P_{gen} to P_{evap} and solving the following set of equations

$$s_{as} = s_{r1} = s\left(T_{gen}, \mathrm{x} = 1\right) \tag{18}$$

$$x_{as} = \frac{s_{as} - s_{f,evap}}{s_{g,evap} - s_{f,evap}} \tag{19}$$

$$h_{as} = h_{f,evap} + \mathrm{x}_{as}\left(h_{g,evap} - h_{f,evap}\right) \tag{20}$$

$$\eta_{nozz} = \frac{h_{r1} - h_a}{h_{r1} - h_{as}} \tag{21}$$

where the subscript as denotes the isentropic state associated with point (a), whereas the subscripts f and g represent the corresponding saturated liquid and saturated vapor states at P_{evap}, respectively. With a nozzle isentropic efficiency $\eta_{nozz} = 0.80$ [20].

The ejector outlet state is then determined from the diffuser compression process using the diffuser efficiency formulation [18,20]. The vapor quality and entropy at state (b) are determined from

$$\mathrm{x}_b = \frac{h_b - h_{f,evap}}{h_{g,evap} - h_{f,evap}} \tag{22}$$

$$\mathrm{x}_b = \frac{(\mathrm{s}_b - \mathrm{s}_{f,evap})}{(\mathrm{s}_{g,evap} - \mathrm{s}_{f,evap})} \tag{23}$$

The isentropic enthalpy at the diffuser outlet, h_{r2s}, is obtained by evaluating the refrigerant enthalpy at the condenser pressure, P_{cond}, while maintaining the entropy at state (b), as given by

$$h_{r2s} = h\,(P_{cond}, s = \mathrm{s}_b) \tag{24}$$

The actual ejector exit enthalpy is then corrected by the diffuser isentropic efficiency:

$$\eta_{diff} = \frac{h_b - h_{r2s}}{h_b - h_{r2}} \tag{25}$$

where $\eta_{diff} = 0.90$ [20]. Eq. (25) serves as the closure relation for the ejector model. Convergence is achieved by comparing the value of h_{r2} obtained from Eq. (25) with that calculated from Eq. (16). When the difference exceeds the prescribed tolerance, the value of μ is updated and the iterative procedure is repeated until agreement is obtained. In the current implementation, Eqs. (16) – (25) are solved simultaneously using EES, which performs the iterative calculations internally. Consequently, μ is not specified as an input parameter but is determined by the ejector model as a function of the operating temperatures (T_{gen}, T_{evap}, T_{cond}) and the two isentropic efficiencies (η_{diff}, η_{nozz}).

3.8. Performance Parameters. To evaluate the thermodynamic performance of the proposed hybrid HDH–ECS, several performance parameters are defined as follows.

Mass ratio (MR): The mass ratio, MR, represents the relationship between the saline feedwater flow rate and the dry-air flow rate and is calculated as

$$MR = \frac{\dot{m}_w}{\dot{m}_{da}} \tag{26}$$

Recovery ratio (RR): The recovery ratio, RR, indicates the proportion of the incoming feedwater that is recovered as distilled water and is defined by

$$RR\,(\%) = 100 \times \frac{\dot{m}_{pw}}{\dot{m}_w} \tag{27}$$

Gained output ratio (GOR): The gained output ratio (GOR) is widely used to assess the thermal performance of HDH desalination systems. It is defined as the ratio between the latent heat associated with the produced freshwater and the total external thermal energy supplied to the system [16]

$$GOR = \frac{\dot{m}_{pw}\, h_{fg}}{\dot{Q}_{gen} + \dot{W}_{pump}} \tag{28}$$

where h_{fg} is the latent heat of vaporization of water, evaluated at T_{pw}.

Coefficient of performance (COP): The coefficient of performance (COP) of the ejector cooling cycle is evaluated as the

ratio of the useful cooling effect generated in the evaporator to the heat supplied to the generator

$$COP = \frac{\dot{Q}_{evap}}{\dot{Q}_{gen} + \dot{W}_{pump}} \tag{29}$$

4. RESULTS AND DISCUSSION

4.1. Input Parameters and Operating Ranges. The developed thermodynamic model of the HDH–ejector cycle was implemented using the governing mass and energy balance equations presented in the previous section. To evaluate the system performance, a set of operating parameters and input ranges was specified, as summarized in Table 1. These parameters were selected to represent the main variables affecting the performance of the integrated system.

4.2. Model Validation. The developed thermodynamic model for the CAOW modified air-heated HDH cycle in which the humid air is first humidified (1→2), then heated in an external heater (2→3), and finally dehumidified to produce distillate (3→1) was validated against the widely cited results of Narayan et al.[4] for the same configuration, using the same boundary temperatures and component effectiveness values reported for the reference cycle assessment.

Table 2 summarizes the principal operating conditions used in the comparison. As shown, the present study adopts the same minimum and maximum temperatures, pressure, and dehumidifier effectiveness used in the reference study. The humidifier effectiveness was varied parametrically to reproduce the reported trend of cycle performance.

Table 1. *Input parameters for the HDH-Ejector cycle system*

Parameter	Symbol	Value	Unit
Mass ratio	MR	0.5–2.5	–
Air relative humidity	ϕ_1 and ϕ_2	1.0	–
Pressure of the system	P	100	kPa
Humidifier efficiency	ε_H	0.90	–
Dehumidifier efficiency	ε_D	0.90	–
Top air temperature	T_{a3}	60–90	°C
Feedwater inlet temperature	T_{W00}	30	°C
Generator temperature	T_{gen}	80–95	°C
Evaporator temperature	T_{evap}	10–25	°C
Condenser temperature	T_{cond}	35–50	°C

Table 2. *Validation conditions for the CAOW modified air-heated HDH cycle*

Parameter	Reference study [4]	Current study
Minimum temperature, T_{min} (°C)	30	30
Maximum temperature, T_{max} (°C)	80	80
Pressure, (P) (kPa)	100	100
Dehumidifier effectiveness, ε_D	0.90	0.90

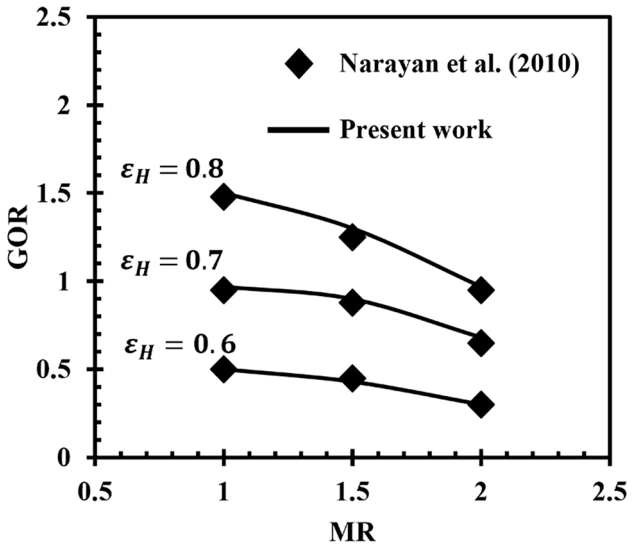

Figure 4. Validation of the CAOW modified air-heated HDH model: predicted GOR versus mass-flow ratio MR for different humidifier effectiveness values (ε_h); $T_{a3} = 80°C$, $T_{w0} = 30°C$, $P = 100$ kPa, $\varepsilon_d = 0.90$

Under the baseline operating conditions ($T_{a3} = 80°C$, $T_{w0} = 30°C, P = 100$kPa, $\varepsilon_D = 0.90$), the predicted cycle-level GOR of the model is 3.474, which is in close agreement with the reported value of 3.5[4], with a deviation of approximately 0.74%, as shown in Figure 4. In addition, the model reproduces the reported parametric behavior: GOR increases with humidifier effectiveness ε_H and decreases with MR, consistent with the reference data[4]. These trends and magnitudes support the correct implementation of the governing balances and component effectiveness in the model.

4.3. HDH Enhanced by ECS. Figure 5 compares the variation of GOR and RR for the standalone CAOW HDH cycle (Figure 1) and the hybrid HDH–ECS configuration (Figure 3) over the investigated range of MR. The comparison was performed at $T_{w00} = 30°C$, $T_{a3} = 60°C$, $P = 100$ kPa, $\varepsilon_H = \varepsilon_D = 0.90$, $T_{gen} = 90°C$, $T_{cond} = 40°C$, and $T_{evap} = 25°C$. As shown in Figure 5(a), the hybrid HDH–ECS configuration yields consistently higher GOR values than the standalone HDH cycle over the entire investigated MR range. For both systems, GOR initially increases with MR, reaches a maximum at $MR = 0.9$, and then decreases as MR increases further. Quantitatively, the hybrid system attains a peak GOR of 5.299, whereas that of the standalone HDH cycle is 3.738 under the same conditions. This corresponds to an enhancement of approximately 41.8%, demonstrating that the integration of the ejector cooling subsystem significantly improves the thermal performance of the HDH cycle.

A different trend is observed for RR in Figure 5(b). At low MR values, the hybrid HDH–ECS system achieves slightly higher RR values than the standalone HDH cycle. The maximum RR of the hybrid system is 3.257% at $MR = 0.7$, whereas that of the standalone cycle is 3.202% at $MR = 0.9$. These values correspond to the baseline comparison case considered in Figure 5(b).

As MR increases beyond the low-MR region, the difference between the two configurations gradually diminishes, and both systems exhibit nearly similar RR values in the intermediate

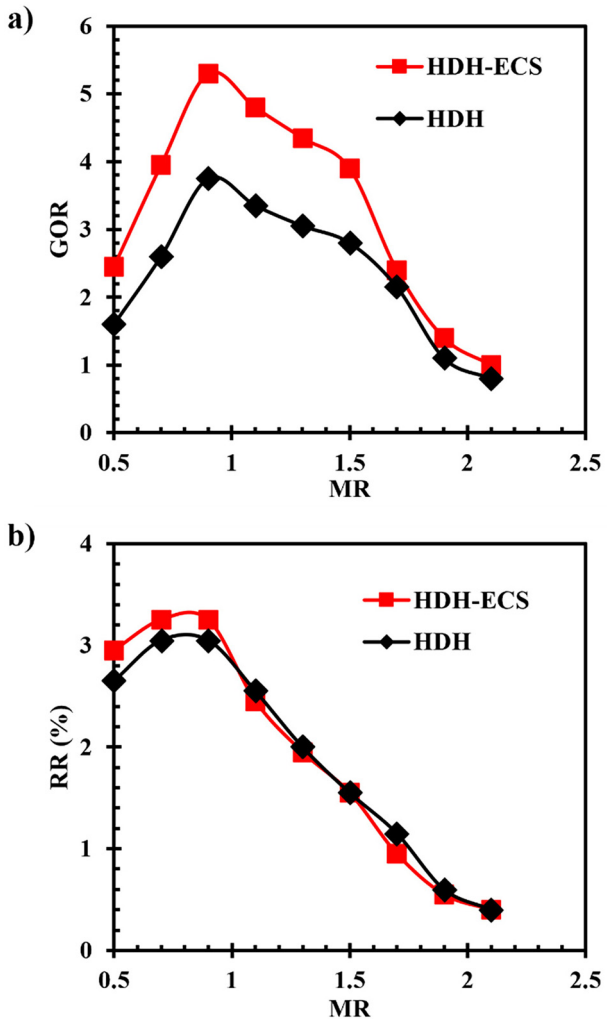

Figure 5. (a) GOR and (b) RR of the basic HDH cycle (Figure 1) compared with those of the HDH–ECS system (Figure 3). The operating conditions are $T_{w00} = 30°C, T_{a3} = 60°C, P = 100\,kPa, \varepsilon_H = \varepsilon_D = 0.90, T_{gen} = 90°C, T_{cond} = 40°C, and\ T_{evap} = 25°C$

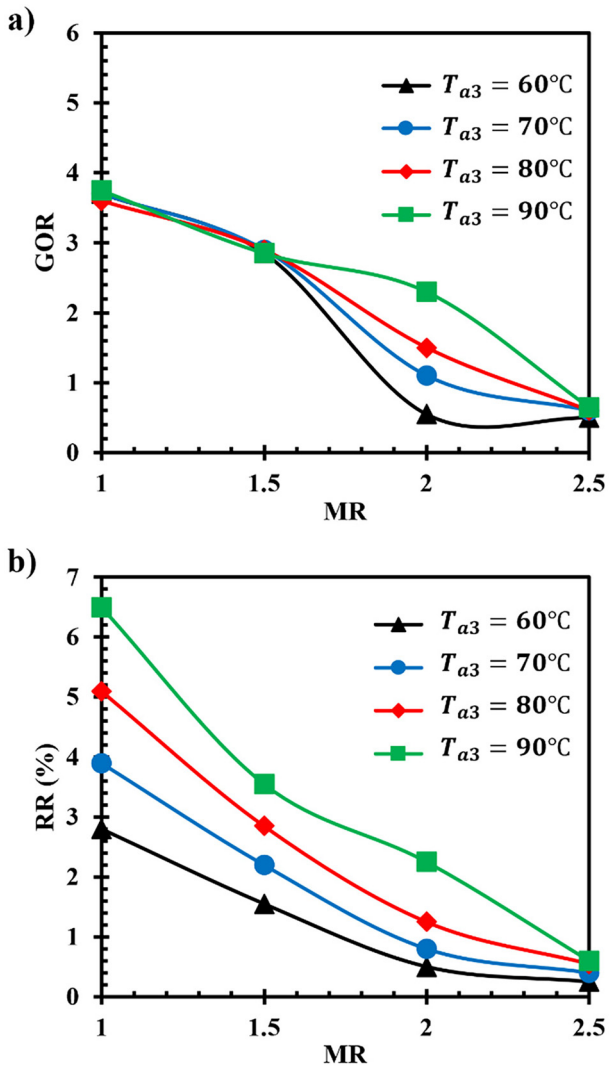

Figure 6. Variation of (a) GOR and (b) RR with mass ratio at different values of T_{a3}, under $T_{w00} = 30°C$, $P = 100$kPa, $\varepsilon_H = \varepsilon_D = 0.90$, $T_{gen} = 90°C$, $T_{cond} = 50°C$, and $T_{evap} = 10°C$

range. At higher MR values, however, the standalone HDH cycle becomes slightly superior to the hybrid configuration. These results indicate that the benefit of the hybrid system is much more pronounced in terms of GOR than RR under the selected operating conditions.

4.4. Effect of Top Temperature T_{a3}. Figure 6(a) presents the variation of GOR with MR at different values of the top air temperature, T_{a3}, ranging from 60°C to 90°C, under the operating conditions of $T_{w00} = 30°C$, $P = 100$Kpa,$\varepsilon_H = \varepsilon_D = 0.90$, $T_{gen} = 90°C$, $T_{cond} = 50°C$, and $T_{evap} = 10°C$. It can be observed that the effect of T_{a3} on the system performance depends strongly on the MR range. At relatively low MR values, GOR is higher for lower top air temperatures, and the highest value within the investigated range is obtained at $T_{a3} = 60°C$, where GOR reaches approximately 3.73 at $MR = 1$. As MR increases to about 1.5, the differences between the curves remain small, although the lower T_{a3} cases still yield slightly better performance. However, a different behavior is observed near $MR = 2$, where the GOR corresponding to higher T_{a3} becomes significantly larger than that at lower T_{a3}. For example, at $MR = 2$, GOR increases from approximately 0.95 at $T_{a3} = 60°C$ to nearly 2.30 at $T_{a3} = 90°C$. Beyond this region, GOR decreases rapidly with further increase in MR for all cases, and the influence of T_{a3} becomes progressively weaker, as all curves converge to relatively low values at high MR. Therefore, the effect of increasing the top air temperature is not monotonic over the entire operating range; rather, its impact is more pronounced in the intermediate MR region, while at high MR the thermal performance of all cases becomes nearly similar.

Figure 6(b) illustrates the variation of RR with MR at different values of the top air temperature, T_{a3}, ranging from 60°C to 90°C, under the operating conditions of $T_{w0} = 30°C$, $P = 100$Kpa,$\varepsilon_H = \varepsilon_D = 0.90$, $T_{gen} = 90°C$, $T_{cond} = 50°C$, and $T_{evap} = 10°C$. As shown, RR decreases monotonically with increasing MR for all investigated values of T_{a3}. RR also increases significantly as T_{a3} increases, with the highest values consistently obtained at $T_{a3} = 90°C$ and the lowest values at $T_{a3} = 60°C$. Within the top-air-temperature parametric study, the maximum RR is approximately 6.44% at $MR = 1$ for $T_{a3} = 90°C$, whereas the corresponding value at $T_{a3} = 60°C$ is approximately 2.78%.

This increase is mainly attributed to the higher top air temperature, which enhances the evaporation rate in the humidifier and consequently increases the amount of condensable water vapor in the dehumidifier. As MR increases, RR drops sharply, particularly in the low-MR region between $MR = 1$ and $MR = 2$, after which the rate of decrease becomes less pronounced. Moreover, the influence of T_{a3} is strongest at low MR values, where the separation between the curves is large, while at higher MR values, the curves gradually converge toward relatively small RR values. This behavior indicates that increasing the top air temperature enhances the water recovery capability of the system, although the beneficial effect becomes progressively weaker as MR increases. The investigated top-air temperature range (60–90°C) is practically achievable using low-grade thermal energy sources such as solar thermal collectors and industrial waste heat, making the proposed system suitable for decentralized desalination applications.

4.5. Effect of Ejector Operating Conditions on GOR and μ. Figure 7 shows the variation of GOR and μ, with (a) generator temperature, T_{gen}, (b) condenser temperature, T_{cond}, and (c) evaporator temperature, T_{evap}, for the hybrid HDH–ECS under the selected operating conditions. As shown in Figure 7(a), increasing T_{gen} from 80 to 100°C produces only a modest improvement in system performance. Over this range, GOR increases gradually from 4.791 to 5.247, while μ rises from 0.4521 to a maximum of 0.5471 at 95°C, followed by a slight decrease to 0.5378 at 100°C. This behavior indicates that increasing T_{gen} strengthens the primary ejector flow and enhances entrainment, but its overall influence remains limited within the investigated range.

The condenser and evaporator temperatures exert a much stronger influence on system performance, as shown in Figures 7(b) and 7(c). Increasing T_{cond} from 35 to 55°C causes a clear deterioration in both GOR and μ; GOR decreases from 5.926 to 3.891, while μ drops sharply from 0.8430 to 0.1264. Physically, a higher T_{cond} increases the condensing pressure and therefore the back pressure imposed on the ejector, which reduces the effective pressure ratio across the device. As a result, the induced secondary mass flow rate is suppressed, leading to lower internal heat recovery and weaker overall performance of the coupled HDH–ejector system.

Increasing T_{evap} strongly enhances both GOR and μ, as illustrated in Figure 7(c). When T_{evap} is raised from 10 to 30°C, GOR increases from 4.092 to 5.802, while μ rises markedly from 0.2062 to 0.7895. This demonstrates that T_{evap} has the most beneficial effect on ejector operation. A higher T_{evap} increases the secondary vapor pressure and reduces the temperature lift required between the evaporator and condenser, improving the mixing process inside the ejector and increasing the refrigeration effect per unit generator heat input. Consequently, a larger fraction of the supplied thermal energy is internally recovered and reused by the HDH cycle.

4.6. Sensitivity Comparison of Ejector Operating Temperatures. Figure 8 summarizes the relative sensitivities of GOR and μ, to variations in the three principal ejector operating temperatures, namely T_{gen}, T_{evap}, and T_{cond}, over the investigated range $\Delta T = 15$°C at $T_{a3} = 60$°C and $T_{w0} = 30$°C. Among the investigated parameters, the evaporator temperature exhibits the strongest influence on system performance. Increasing T_{evap} from 10 to 25°C increases GOR from 4.092 to 5.024, corresponding to a variation of 22.78%, while the entrainment ratio rises markedly from 0.2062 to 0.5256, giving a variation of 154.90%. This strong sensitivity indicates that T_{evap} plays a dominant role in enhancing the secondary vapor pressure and improving the entrainment capability of the ejector.

The condenser temperature is the second most influential parameter, but with an opposite effect on performance. Increasing T_{cond} from 35 to 50°C reduces GOR from 5.926 to 4.144, corresponding to a variation of 30.07%, while μ decreases from 0.8430 to 0.2159, corresponding to a variation of 74.39%. This behavior is attributed to the increase in condensing pressure, which raises the back pressure on the ejector and weakens the induced secondary flow. The generator temperature has the weakest effect within the investigated range. Increasing T_{gen} from 80 to 95°C increases GOR from 4.791 to 5.130, corresponding to a variation of 7.08%, while μincreases from 0.4521 to 0.5471, corresponding to a variation of 21.01%. These results confirm that effective control of T_{evap} and T_{cond} is more critical for improving the hybrid system performance than further increasing T_{gen}, which provides only limited additional benefit over the selected interval. From a practical perspective, the results suggest that maintaining a high evaporator temperature and a low

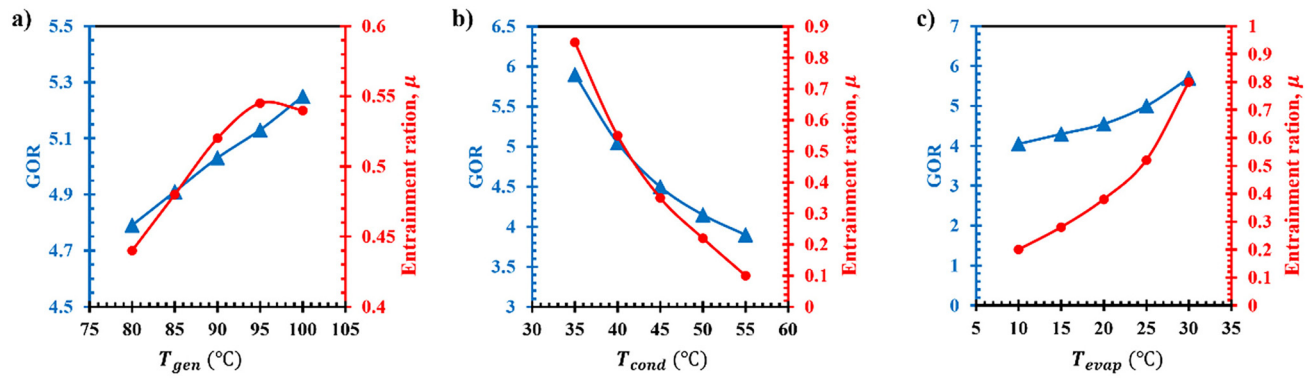

Figure 7. Variation of the GOR and entrainment ratio, μ, with (a) generator temperature, T_{gen}, (b) condenser temperature, T_{cond}, and (c) evaporator temperature, T_{evap}, for the hybrid HDH–ejector cooling system under the selected operating conditions at $T_{a3} = 60°C$ and $T_{w00} = 30°C$

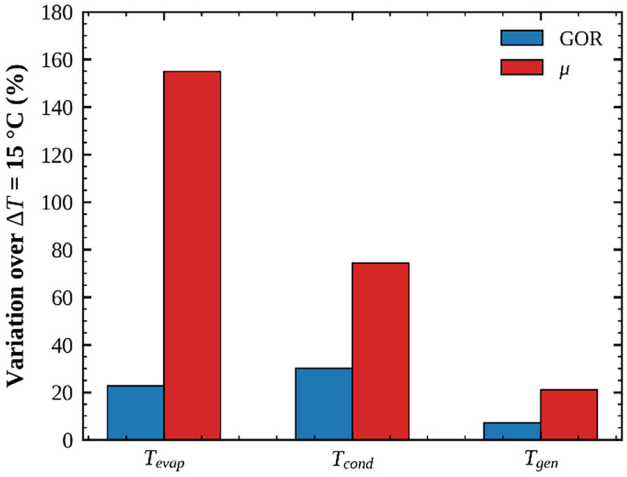

Figure 8. Sensitivity comparison of the effects of T_{gen}, T_{evap}, and T_{cond} on GOR and entrainment ratio, μ, over the investigated range $\Delta T = 15°C$ at $T_{a3} = 60°C$ and $T_{w00} = 30°C$

condenser temperature is essential for maximizing system performance. This can be achieved through effective heat-source management and adequate condenser cooling, particularly in decentralized desalination systems utilizing low-grade thermal energy.

4.7. Comparison with Published Studies. To further evaluate the significance of the results, the performance of the proposed HDH–ECS system was compared with the performance of selected HDH-based and hybrid desalination systems reported in the literature, as summarized in Table 3. The selected studies were limited to systems that report GOR or GOR improvement, allowing a more consistent comparison with our results. Since the compared systems differ in configuration, heat source, working fluid, operating conditions, and system boundaries, the comparison is intended to provide a qualitative performance benchmark rather than a direct one-to-one evaluation. Nevertheless, it helps clarify the performance level of the proposed configuration relative to that of conventional and hybrid HDH-based desalination systems.

Table 3 show that the proposed system achieves a higher GOR than the reference CAOW HDH configuration reported by Narayan et al.[4] and the previously investigated water-heated HDH–ECS system[16]. Al-Mahmoud et al.[13] also reported a 20% improvement in GOR for a hybrid HDH–ejector refrigeration system, while Ali et al.[14] reported a GOR of 2.75 for a solar-powered ejector-assisted adsorption desalination–HDH system. Compared with these studies, the proposed configuration directly couples the ejector condenser with the closed air loop and uses the ejector evaporator to precool the feedwater entering the dehumidifier. This dual thermal interaction improves internal heat recovery and enhances the condensation driving potential. Although differences in configurations and operating conditions prevent direct one-to-one comparisons, the proposed CAOW HDH–ECS system demonstrates competitive thermal performance among HDH-based hybrid desalination systems.

Beyond the HDH-based systems listed in Table 3, the proposed configuration can be qualitatively compared with mature desalination technologies such as reverse osmosis (RO) and multi-effect distillation (MED). RO is widely recognized as one of the most energy-efficient large-scale seawater desalination technologies, with typical specific energy consumption values of approximately 2–4 kWh/m^{3}for modern seawater RO systems[21]. However, RO relies mainly on electrical energy, high-pressure operation, and membrane pretreatment. MED, in contrast, is a thermal desalination process commonly evaluated using GOR; a recent MED-based system reported a GOR of about 3.69, depending on the heat source and operating configuration[22]. The proposed HDH–ECS system is not intended to replace large-scale RO or MED plants; rather, it targets small-scale and decentralized applications where low-grade thermal energy is available. Its main advantage is the enhancement of conventional HDH thermal efficiency through ejector-assisted internal heat recovery, achieving a GOR of 5.3 in this study.

4.8. Study Limitations. This study provides a steady-state thermodynamic assessment of the proposed HDH–ECS configuration. Accordingly, the analysis is limited by the assumptions of negligible heat losses and pressure drops, idealized component behavior, and fixed operating conditions. The scope of this study excluded detailed ejector geometry, transient operation under variable solar or waste-heat input, experimental validation, exergy analysis, environmental assessment, and techno-economic assessment. Future work should prioritize experimental validation and techno-economic assessment, followed by exergy and environmental analyses, to further evaluate the practical feasibility and commercialization potential of the proposed system.

Table 3. *Comparison of the proposed HDH–ECS system with selected published HDH-based systems*

Study	System configuration	Main feature	Reported GOR / performance	Remarks
Narayan et al.[4]	CAOW HDH cycle	Modified air-heated HDH cycle	GOR = 3.5	Validation reference
Al-Mahmoud et al.[13]	HDH + ejector refrigeration cycle	Water-heated HDH	GOR improved by 20%	Hybrid desalination/cooling
Ali et al.[14]	Adsorption desalination–HDH system	Solar-powered system with two ejectors	GOR = 2.75	Ejector-assisted hybrid system
Munteshari[16]	HDH + ejector cooling system	Water-heated HDH, R141b	GOR up to 4.5	42% GOR enhancement
Present study	CAOW HDH + ECS	Air-heated HDH, R134a	GOR = 5.3	41.8% GOR enhancement

5. CONCLUSION

This study proposed and thermodynamically analyzed a CAOW HDH desalination system integrated with a thermally driven R134a ECS. In the proposed configuration, the ejector condenser replaces the conventional external air heater, while the ejector evaporator precools the feedwater entering the dehumidifier. The main conclusions are summarized as follows:

- The proposed HDH–ECS system achieved a peak GOR of 5.3, compared with 3.7 for the standalone HDH cycle under the same baseline conditions—a thermal performance enhancement of approximately 41.8%.
- The maximum recovery ratio of the hybrid system reached 3.257% at MR = 0.7, while the standalone HDH cycle achieved a maximum recovery ratio of 3.202% at MR = 0.9. This indicates that the improvement in recovery ratio is limited compared with the improvement in GOR.
- The effect of top air temperature, T_{a3}, depends strongly on MR. At low MR, lower T_{a3} produced higher GOR values. However, at higher MR, increasing T_{a3} improved GOR. The recovery ratio increased consistently with T_{a3}, reaching a maximum value of approximately 6.44% at T_{a3} = 90°C and MR = 1.
- The ejector entrainment ratio, μ, was found to be a key parameter controlling the thermal performance of the integrated system. A higher entrainment ratio improved internal heat recovery and enhanced the overall GOR.
- Among the ejector operating temperatures, the evaporator temperature had the strongest positive effect. Increasing T_{evap} from 10 to 30°C increased GOR from 4.092 to 5.802 and increased μ from 0.2062 to 0.7895.
- The condenser temperature had a strong negative effect on performance. Increasing T_{cond} from 35 to 55°C reduced GOR from 5.926 to 3.891 and μ from 0.8430 to 0.1264.
- The generator temperature had the weakest effect among the ejector operating temperatures. Increasing T_{gen} from 80 to 100°C increased GOR only from 4.791 to 5.247, while μ increased from 0.4521 to 0.5378.
- The results indicate that controlling T_{evap} and T_{cond} is more important for improving system performance than further increasing T_{gen}.

Overall, the proposed HDH–ECS configuration demonstrates a practical approach for improving the thermal efficiency of small-scale desalination systems utilizing low-grade thermal energy sources and may be particularly suitable for decentralized desalination applications powered by renewable or waste-heat resources.

AFFILIATIONS AND AUTHOR DETAILS

Undergraduate Author

Rand Almutairi – *Department of Mechanical Engineering, King Fahd University of Petroleum & Minerals, Dhahran 31261, Saudi Arabia*; 0009-0009-2662-0156
Email: randsa00@gmail.com

Corresponding Author

Obaidallah Munteshari – *Research Mentor, Assistant Professor, Department of Mechanical Engineering, King Fahd University of Petroleum & Minerals, Dhahran 31261, Saudi Arabia*; 0000-0003-3587-4632
Email: obaidallah@kfupm.edu.sa

REFERENCES

(1) Th e 2030 Water Resources Group, *Charting Our Water Future: Economic frameworks to inform decision-making*, 2009. [Online]. Available: https://www.2030wrg.org/publication/charting-our-water-future/. [Accessed: Oct. 23, 2025].

(2) International Energy Agency (IEA), *Global Energy Review 2025*, Mar. 2025. [Online]. Available: https://www.iea.org/reports/global-energy-review-2025. [Accessed: Oct. 23, 2025].

(3) D. U. Lawal and N. A. A. Qasem, "Humidification-dehumidification desalination systems driven by thermal-based renewable and low-grade energy sources: A critical review," *Renewable and Sustainable Energy Reviews*, vol. 125, p. 109817, Jun. 2020, doi: 10.1016/j.rser.2020.109817.

(4) G. P. Narayan, M. H. Sharqawy, J. H. Lienhard V, and S. M. Zubair, "Thermodynamic analysis of humidification–dehumidification desalination cycles," *Desalination and Water Treatment*, vol. 16, no. 1–3, pp. 339–353, Apr. 2010, doi: 10.5004/dwt.2010.1078.

(5) R. Xiong, S. Wang, and Z. Wang, "A mathematical model for a thermally coupled humidification–dehumidification desalination process," *Desalination*, vol. 196, no. 1–3, pp. 177–187, Sep. 2006, doi: 10.1016/j.desal.2006.01.012.

(6) S. Farsad and A. Behzadmehr, "Analysis of a solar desalination unit with humidification–dehumidification cycle using DoE method," *Desalination*, vol. 278, no. 1–3, pp. 70–76, Sep. 2011, doi: 10.1016/j.desal.2011.05.008.

(7) A. Mahmoudi, M. S. Valipour, and S. Rashidi, "Performance enhancement techniques in humidification–dehumidification desalination systems: A detailed review," *Journal of Thermal Analysis and Calorimetry*, vol. 150, pp. 8413–8442, 2025, doi: 10.1007/s10973-024-13489-7.

(8) M. Ziauddin, F. Alnaimat, and B. Mathew, "A novel humidification and dehumidification desalination system powered by direct solar energy," *Case Studies in Thermal Engineering*, vol. 72, Art. no. 106236, 2025, doi: 10.1016/j.csite.2025.106236.

(9) S. He, Y. Li, and R. Z. Wang, "Progress of mathematical modeling on ejectors," *Renewable and Sustainable Energy Reviews*, vol. 13, no. 8, pp. 1760–1780, Oct. 2009, doi: 10.1016/j.rser.2008.09.032.

(10) N. Khaldi, S. Sdiri, and M. Lazaar, "Thermodynamic analysis and optimization of an ejector refrigeration system for sustainable cooling applications," *International Journal of Refrigeration*, vol. 174, pp. 372–387, Jun. 2025, doi: 10.1016/j.ijrefrig.2025.03.004.

(11) M. Khennich, N. Galanis, M. Sorin, J. Orfi, A. Sarrafi, and S. Dupuis, "Thermodynamic analysis of a solar powered ejector cooling system," *International Journal of Thermofluids*, vol. 24, Nov. 2024, Art. no. 100960, doi: 10.1016/j.ijft.2024.100960.

(12) V. K. Yadav, J. Sarkar, and P. Ghosh, "Recent advances and future outlook on solar-powered ejector refrigeration and associated multi-generation systems," *Journal of Thermal Analysis and Calorimetry*, vol. 149, pp. 7869–7889, 2024, doi: 10.1007/s10973-024-13311-4.

(13) H. A. Al-Mahmoud, N. I. Ibrahim, F. A. Al-Sulaiman, and S. M. Zubair, "Thermodynamic performance evaluation of a hybrid ejector cooling and humidification–dehumidification desalination system," *Energy Conversion and Management*, vol. 225, Dec. 2020, Art. no. 113450, doi: 10.1016/j.enconman.2020.113450.

(14) E. S. Ali, A. S. Alsaman, R. Ben Mansour, and R. Ben-Mansour, "Techno-economic and environmental assessment of solar-driven hybrid adsorption desalination–HDH using silica gel/CaCl2 under Saudi Arabian climate," *Gels*, vol. 12, no. 3, Art. no. 226, 2026, doi: 10.3390/gels12030226.

(15) A. E. Kabeel, M. A. Elazab, M. R. Diab, E. M. S. El-Said, M. El Hadi Attia, and M. K. Elshaarawy, "Hybrid humidification-dehumidification with renewable energy integration for enhanced desalination: An overview," *Renewable and Sustainable Energy Reviews*, vol. 211, p. 115313, 2025, doi: 10.1016/j.rser.2024.115313.

(16) O. Munteshari, "Thermodynamic analysis of a novel humidification–dehumidification desalination system enhanced by a thermally driven ejector cooling system," *Case Studies in Thermal Engineering*, vol. 77, p. 107570, 2026.

(17) H. J. Xu, S. C. Jiang, M. Xie, T. Jia, and Y. Dai, "Technical improvements and perspectives on humidification-dehumidification desalination — A review," *Desalination*, vol. 541, p. 116029, 2022, doi: 10.1016/j.desal.2022.116029.

(18) G. K. Alexis and E. D. Rogdakis, "A verification study of steam-ejector refrigeration model," *Applied Thermal Engineering*, vol. 23, no. 1, pp. 29–36, 2003, doi: 10.1016/S1359-4311(02)00116-3.

(19) J. T. Munday and D. F. Bagster, "A New Ejector Theory Applied to Steam Jet Re frigeration", Industrial & Engineering Chemistry Process Design and Development, vol. 16, no. 4, pp. 442–449, 10 1977.

(20) G.K. Alexis and E.K. Karayiannis, "A solar ejector cooling system using refrigerant R134a in the Athens area", Renewable Energy, vol. 30, no. 9, pp. 1457–1469, 7 2005.

(21) M. Elimelech and W. A. Phillip, "The future of seawater desalination: Energy, technology, and the environment," *Science*, vol. 333, no. 6043, pp. 712–717, 2011, doi: 10.1126/science.1200488.

(22) M. Haqiqi, S. Dussi, and J. C. Garcia-Navarro, "Multi-effect distillation for water desalination in an offshore PEM electrolyser system," *Energy Reports*, vol. 14, pp. 1452–1466, Dec. 2025, doi: 10.1016/j.egyr.2025.07.031.